# Convective chemical fronts in a Poiseuille flow

Desiderio A. Vasquez*
*Departamento de Ciencias, Sección Física, Pontificia Universidad Católica del Perú, Apartado 1761, Lima, Peru*
(Received 18 August 2007; published 12 November 2007)

Autocatalytic reaction fronts propagating in a Poiseuille flow present a change of speed and curvature depending on the strength of the flow and on the direction of front propagation. These chemical fronts separate reacted and unreacted fluids of different densities, consequently convection will always be present due to the horizontal density gradient of the curved front. In this paper, we find the change of speed caused by gravity for fronts propagating in vertical tubes under a Poiseuille flow. For small density differences, we find axisymmetric fronts. Our theory predicts a transition to nonaxisymmetric fronts as the distance between the walls is increased. The transition depends on the average speed of the Poiseuille flow.

DOI: 10.1103/PhysRevE.76.056308 PACS number(s): 47.20.Bp, 82.40.Ck, 47.70.Fw

## I. INTRODUCTION

Chemical reactions such as the Belousov-Zhabotinsky reaction [1], the chlorite-tetrathionate (CT) reaction [2–4], the iron(II)-nitric acid system [5], the iodate-sulfate system [6], and the iodate-arsenous acid reaction [7–10] exhibit waves of chemical activity that separate regions of different chemical concentrations. Such chemical waves generate thermal and compositional gradients leading to mass density gradients. These density gradients can cause convective fluid motion for reactions taking place in aqueous solutions. Several theoretical and experimental studies have established conditions for convective fluid motion in chemical fronts [11–21].

Experiments in the iodate-arsenous acid reaction in vertical tubes showed a transition to convective fronts as the diameter of the tube was increased [7,8]. Convection only occurs in fronts propagating upward since the unreacted fluid is heavier than the reacted fluid. This reaction exhibits flat fronts without convection and also nonaxisymmetric and axisymmetric fronts with convection, depending on the tube diameter. The change in curvature of the front due to convection is accompanied by an increase in front speed. This transition was predicted by a theoretical analysis that considered the front as a thin boundary between two fluids of different densities [22]. Thermal effects were included considering the limit of infinite thermal diffusivity. In Hele-Shaw cells, where the fluid is confined between two planar walls, fronts in the iodate reaction develop fingers caused by the convective fluid motion. Detailed experiments with this reaction measured the dispersion relation between the growth rate and the wavelength of small perturbations to the flat convectionless front [9,10]. Good agreement between theory and experiment were also found for fronts in the CT reaction in Hele-Shaw cells [2,3]. In this case, the reacted fluid is heavier than the unreacted fluid, consequently convection sets in for downward propagating fronts. More recent experiments showed a chemical plume propagating upward in the iodate-arsenous acid reaction having shape and speed characterized by convective fluid motion [23].

Recent experimental and theoretical work analyzed the interaction between chemical wave propagation with an imposed external fluid flow. Edwards [24] predicted the change of speed for fronts in the iodate-arsenous acid reaction as they propagate in the same or opposing direction of a Poiseuille flow. This work showed that for large gaps an adverse Poiseuille flow would not have large effects in the front speed. Experiments by Salin *et al.* in cylindrical tubes and Hele-Shaw cells verified this effect, as well as the cusplike shape exhibited by these fronts [25]. The theoretical understanding of chemical fronts under an external fluid flow has not included gravitational effect caused by density gradients. Since the imposed Poiseuille flow deforms the flat front, convective fluid motion should always be present due to a horizontal density gradient. In this work we analyze the effects of convective fluid motion for fronts in Poiseuille flows. We will couple the Navier-Stokes equations describing viscous fluid motion to the reaction-diffusion equation that describes the chemical wave propagation. We will show how these effects can also be obtained using an eikonal relation between the front curvature and the normal speed of propagation. Experiments can be designed to test these predictions.

## II. EQUATIONS OF MOTION

We model the propagation of the chemical front by coupling the reaction-diffusion equation describing the autocatalytic front in a moving fluid with $\vec{V}$ as the velocity [26–29],

$$\frac{\partial a}{\partial t} + \vec{V} \cdot \vec{\nabla} a = D\nabla^2 a - k_c a(a_0 - a)^2. \tag{1}$$

Here we use a third order autocatalysis for the concentration $a$ that applies to fronts in the iodate-arsenous acid reaction. The parameter $a_0$ is the concentration of the unreacted fluid. We set the front to propagate upward in a two-dimensional slab, where the horizontal direction $x$ is confined by two vertical walls at $x=0$ and $x=a$. The vertical $z$ direction has horizontal boundaries far away from the front. The velocity field arises from a Poiseuille flow imposed on a fluid of variable density. A diagram showing the front propagating in a fluid of constant density can be found in Edwards [24].

*Permanent address: Department of Physics, Indiana University Purdue University Fort Wayne, Fort Wayne, IN 46805.

 

We use the Navier-Stokes equations in the Bousinesque approximation, where the changing density affects only the large gravity term,

$$\frac{\partial \vec{V}}{\partial t} + (\vec{V}\cdot\vec{\nabla})\vec{V} = -\frac{1}{\rho_0}\vec{\nabla}P + \nu\nabla^2\vec{V} - \frac{\rho}{\rho_0}g\hat{z}. \tag{2}$$

Here $P$ is the pressure, $\rho$ is the mass density of the fluid, $\rho_0$ is the mass density of the unreacted fluid, $\nu$ is the kinematic viscosity, $g$ is the magnitude of the acceleration of gravity, and $\hat{z}$ is a unit vector in the direction upward of the gravity.

In this approximation the continuity equation is reduced to

$$\vec{\nabla}\cdot\vec{V} = 0. \tag{3}$$

We will solve the equations in the two dimensional $x$-$z$ plane. The continuity equation allows us to write the fluid equations in terms of the stream function-vorticity ($\psi$) and the vorticity ($\omega$) defined as

$$V_x = \frac{\partial\psi}{\partial z}, \quad V_z = -\frac{\partial\psi}{\partial x}, \tag{4}$$

and

$$\nabla^2\psi = \omega. \tag{5}$$

With this definition the Navier-Stokes equations are written as

$$\frac{\partial\omega}{\partial t} = \frac{\partial(\psi,\omega)}{\partial(x,z)} + \nu\nabla^2\omega + \frac{g}{\rho_0}\frac{\partial\rho}{\partial x}. \tag{6}$$

For two functions $f_1$ and $f_2$ we defined

$$\frac{\partial(f_1,f_2)}{\partial(x,z)} = \frac{\partial f_1}{\partial x}\frac{\partial f_2}{\partial z} - \frac{\partial f_1}{\partial z}\frac{\partial f_2}{\partial x}. \tag{7}$$

We write the equations of motion in dimensionless form using $t_{ch}=(k_c a_0^2)^{-1}$ as unit of time, $L=(Dt_{ch})^{1/2}$ as unit of length, $D$ as unit of the stream function, $D/L^2$ as unit of the vorticity, the dimensionless concentration $c=a/a_0$,

$$\frac{\partial\omega}{\partial t} = \frac{\partial(\psi,\omega)}{\partial(x,z)} + \mathrm{S}_c\nabla^2\omega + \mathrm{RaS}_c\frac{\partial c}{\partial x}, \tag{8}$$

and

$$\frac{\partial c}{\partial t} = \frac{\partial(\psi,c)}{\partial(x,z)} + \nabla^2 c - c(1-c)^2. \tag{9}$$

We defined a dimensionless Rayleigh number

$$\mathrm{Ra} = \frac{g\,\delta L^3}{\nu D} \tag{10}$$

and a dimensionless Schmidt number

$$S_c = \frac{\nu}{D}. \tag{11}$$

The parameter $\delta$ represents the fractional density difference between the unreacted fluid and the reacted fluid. We assumed that the density varies linearly with the concentration $c$. For fronts in the iodate-arsenous acid reaction, the Schmidt number is large, we will replace Eq. (8) in the limit of infinite Schmidt number [29],

$$\nabla^2\omega + \mathrm{Ra}\frac{\partial c}{\partial x} = 0. \tag{12}$$

For thin fronts (as in the iodate-arsenous acid reaction) we can replace the reaction-diffusion-advection relation [Eq. (1)] by an eikonal relation between the normal front velocity $v_n$, the flat front speed $v_0$, and the front curvature $\kappa$ (in dimensioned form) [14,30,31],

$$v_n = v_0 + D\kappa + \vec{V}\cdot\hat{n}. \tag{13}$$

Here $\hat{n}$ is a unit vector in the direction normal to the front. In our choice of dimensionless units $v_0$ corresponds to $1/\sqrt{2}$ and $D$ becomes the number 1 as in Ref. [32]. In this case the thin front separates reacted and unreacted fluid. The eikonal relation has shown very good agreement with experiments in locating the onset of convection for autocatalytic fronts. Useful insights will be gained by comparing the solutions of the eikonal relation and reaction-diffusion models. In this paper we will apply it only to fronts of small curvature [33], were the eikonal relation can be written as

$$\frac{\partial H}{\partial t} = v_0 + \frac{\partial^2 H}{\partial x^2} + \left(\frac{v_0}{2}\right)\left(\frac{\partial H}{\partial x}\right)^2 + V_z|_H. \tag{14}$$

Here $z=H(x,t)$ provides the position of the front as a function of the horizontal coordinate $x$. The vertical component of the fluid velocity $V_z|_H$ is evaluated at the front.

In this paper we study the gravitational effects on a chemical front under Poiseuille flow, therefore the fluid velocity will be considered as the Poiseuille flow velocity plus an additional velocity. The fluid velocity for Poiseuille flow corresponds to fluid motion in the vertical $z$ direction with parabolic profile in the horizontal $x$ direction: $V_z^{(0)}(x) = 6\bar{V}x(a-x)/a^2$. Here $\bar{V}$ corresponds to the average fluid velocity. We write the stream function $\psi$ as the sum of the stream function for the Poiseuille flow $\psi_0$ plus the stream function for the additional velocity $\psi'$. The primed stream function satisfies viscous boundary conditions at the wall, $\psi' = \partial_z\psi' = 0$. After making the corresponding substitutions in the dynamic equations we drop the prime on the additional stream function. We point out that in the limit of infinite Schmidt number, Eq. (12) remains unchanged after this substitution. The front evolution equation [Eq. (14)] corresponds to the original equation with the simple addition of the Poiseuille fluid velocity.

## III. FRONT EVOLUTION EQUATION

We study the front evolution equation, Eq. (14), which is the small curvature approximation to the eikonal relation. Previous work using this equation showed good agreement with experiments near the transition to convection without a Poiseuille flow [8,14,15]. This equation also provides a good description for the change in curvature and increase of speed near the onset of convection in vertical tubes [34]. We use

this model to describe the effects of the Poiseuille flow on the convective fronts. The front evolution equation is coupled to Eqs. (5) and (12) describing fluid motion. We begin studying the case of "free" boundaries for the additional flow velocity. Here we only require the additional normal velocity to vanish, which in terms of the stream function leads to the conditions $\psi=\partial_x^2\psi=0$. Free boundaries provide a simple example of the mathematical methods applied. These results can be compared with previous calculations without Poiseuille flow with the same boundary conditions [35].

Under the thin front approximation, the density difference changes abruptly across the front

$$\rho = \rho_0 + \Delta\rho\Theta(z-H). \tag{15}$$

Here $\Theta(y)$ is the step function, 0 if $y\leqslant 0$ and 1 if $y>0$. Substituting into Eq. (12) we find

$$\nabla^2\nabla^2\psi = \mathrm{Ra}\frac{\partial H}{\partial x}\delta(z-H), \tag{16}$$

which is replaced by the equation $\nabla^2\nabla^2\psi=0$ with jump conditions across the front $[\psi]=[\partial_z\psi]=[\partial_z^2\psi]=0$, and $[\partial_z^3\psi]=\mathrm{Ra}\,\partial H/\partial x$. The jump conditions, indicated by the brackets, correspond to the value of $\psi$ just above the front in the unreacted fluid minus the value of $\psi$ just below the front in the reacted fluid. For small curvature fronts, the jump conditions can be evaluated at the average front height neglecting any dependence in the horizontal ($x$) coordinate [35]. Therefore knowing $H$ at a given time, Eq. (16) will give $\psi$. We introduce the corresponding Fourier expansions of $\psi$ and $H$,

$$\psi = \sum_n \psi_n(z)\sin(nqx), \tag{17}$$

and

$$H = \sum_n H_n(z)\cos(nqx), \tag{18}$$

with $q=\pi/a$ and $0\leqslant x\leqslant a$. After substitution into Eq. (16) and projecting over the Fourier expansion, we have the equations for the Fourier coefficients,

$$\frac{d^4\psi_n}{dz^4} - 2(nq)^2\frac{d^2\psi_n}{dz^2} + (nq)^4\psi_n = 0, \tag{19}$$

$$[\psi_n] = \left[\frac{d\psi_n}{dz}\right] = \left[\frac{d^2\psi_n}{dz^2}\right] = 0, \tag{20}$$

and

$$\left[\frac{d^3\psi_n}{dz^3}\right] = -\mathrm{Ra}(nq)H_n. \tag{21}$$

The solution for these equations that vanish far away from the front are

$$\psi_n(z) = \begin{cases} A_n(e^{-nqz} + nqze^{-nqz}) & \text{if } z>0 \\ A_n(e^{nqz} + nqze^{nqz}) & \text{if } z\leqslant 0 \end{cases}. \tag{22}$$

Here we define

$$A_n = -\frac{\mathrm{Ra}H_n}{4(nq)^2}. \tag{23}$$

We introduce this result into the front evolution equation Eq. (14) leading to

$$\frac{\partial H}{\partial t} = v_0 + \frac{\partial^2 H}{\partial x^2} + \left(\frac{v_0}{2}\right)\left(\frac{\partial H}{\partial x}\right)^2 + \frac{\mathrm{Ra}}{4}\sum_n \frac{H_n}{nq}\cos(nqx) + V_z^{(0)}(x). \tag{24}$$

Here $V_z^{(0)}(x)$ corresponds to the $z$ component of the Poiseuille flow with average fluid speed $\bar{V}$. Using the Fourier series for the front height $H$ as given by Eq. (18) we find the time evolution for the Fourier coefficients as a set of ordinary differential equations,

$$\frac{dH_0}{dt} = v_0 + \bar{V} + v_0\frac{q^2}{4}\sum_{n=1} n^2 H_n \tag{25}$$

and

$$\frac{dH_p}{dt} = V_p + \left(-p^2q^2 + \frac{\mathrm{Ra}}{4pq}\right)H_p + v_0\frac{q^2}{4}\sum_{n=1}\sum_{m=1} nmH_nH_m(\delta_{p,|n-m|} - \delta_{p,n+m}) \quad \text{for } p\geqslant 1. \tag{26}$$

Here $V_p$ corresponds to the Fourier coefficient of the Poiseuille flow as in

$$V_z^{(0)}(x) = \sum_{p=0} V_p\cos(pqx) \tag{27}$$

with

$$V_p = \begin{cases} -24\bar{V}/(p^2\pi^2) & \text{for } p \text{ even} \\ 0 & \text{for } p \text{ odd} \end{cases}. \tag{28}$$

Thus the time evolution of the front is defined by the evolution of the Fourier coefficients of the front height $H$ determined by Eq. (26).

A solution for rigid boundary conditions can be found by expanding the stream function in terms of orthogonal eigenfunctions of the operator $d^4/dx^4$, with the eigenfunction and its derivative vanishing at the walls. The front height is still expanded by a Fourier series. This approach gave good agreement with experiments without external flow, even for a one- or two-term truncation [15]. In this paper we will limit ourselves to using a two-term expansion for the stream function, thus we will write

$$\psi(x,z) = \phi_1(z)C_1(x/a-1/2) + \phi_2(z)S_1(x/a-1/2), \tag{29}$$

where the functions $C_1$ and $S_1$ are the corresponding eigenfunctions defined in Chandrasekhar [36]. These expansions are replaced in Eq. (16) and projected over the orthogonal eigenfunctions, leading to a set of equations similar to Eq. (19),

$$\frac{d^4\phi_n}{dz^4} - (g_n/a^2)\frac{d^2\phi_n}{dz^2} + (\lambda_n/a^4)\phi_n = 0. \quad (30)$$

Here $\lambda_n$ is the corresponding eigenvalue, while $g_n$ is calculated using the projection leading to $g_1=12.302\,618\,67$ and $g_2=46.050\,120\,33$. The solution follows the method outlined for free boundaries repeating similar calculations. While we keep two terms in the stream function, we require three terms for the front height truncation, Eq. (18). For these truncations we find the following set of differential equations:

$$\frac{dH_0}{dt} = v_0 + \bar{V} + v_0\frac{q^2}{4}H_1^2 + v_0 q^2 H_2^2, \quad (31)$$

$$\frac{dH_1}{dt} = -q^2 H_1 + v_0 q^2 H_1 H_2 + f_1\frac{\mathrm{Ra}}{q}H_1, \quad (32)$$

and

$$\frac{dH_2}{dt} = -4q^2 H_2 - \frac{v_0}{4}q^2 H_1^2 + f_2\frac{\mathrm{Ra}}{q}H_2 - 6\bar{V}/\pi^2. \quad (33)$$

The values for the parameters $f_i$ are $f_1=0.080\,932\,627$ and $f_2=0.065\,310\,740\,21$ for viscous boundary conditions. For the case of free boundaries, the corresponding truncation of Eq. (26) gives $f_1=1/4$ and $f_2=1/8$.

## IV. THE REACTION-DIFFUSION-CONVECTION EQUATIONS

Our results using the front evolution equations are compared to numerical solutions of the reaction-diffusion-convection system. We used a finite difference method to approximate the spatial derivatives using a rectangular mesh. The time evolution equation is obtained by using a simple Euler method with a very small time step in order to avoid numerical instabilities in the advective term. We solve the discretized Poisson equation [Eq. (5)] to obtain the stream function using the GENBUN subroutine from the FISHPACK software package [37]. The second Poisson equation [Eq. (16)] is also solved using the same method. The implementation of boundary conditions is straightforward for slip boundaries using $\psi=\omega=0$ at the walls. For nonslip boundaries we use $\psi=0$ and $\omega_{1,j}=2\psi_{2,j}/\Delta x^2$ for the left wall, with a similar expression for the right wall [38,39]. We use a self-consistent relaxation technique to obtain the stream function $\psi$, since its value depends on $\omega$ which depends on $\psi$ near the walls [39]. We use a $40\times200$ grid with spacing $\Delta x=\Delta y=0.5$. This reproduces the flat front speed and matches results for previous studies on the transition to convection [26,27]. We let the front evolve from initial conditions with random noise. We shift it backward as it approaches the upper end of the domain. In this way the front achieves propagation with constant speed.

## V. RESULTS

We study solutions to the reaction-diffusion-convection equations and compare them with results from the thin front approximation. We establish the regime of interest by choosing appropriate initial values for the parameters that define the front propagation. According to our dimensionless units, the front propagation depends on the Rayleigh number (Ra), the dimensionless distance between the walls ($a$), and the dimensionless average Poiseuille flow ($\bar{V}$). In our units, the time scale is determined by the reaction kinetics. Using the results of Saul and Showalter [40] for fronts in the iodate-arsenous acid reaction described by a cubic equation, we estimate a chemical time $t_{ch}=1.1594$ s. We found the corresponding length scale using a diffusion coefficient of $D=2\times10^{-5}$ cm/s$^2$ as in Wu [26], resulting in $L=4.815\times10^{-3}$ cm. According to experiments in vertical cylinders, the transition to convection in fronts in the iodate arsenous acid reaction occurs near a diameter of $d_c=0.92$ mm, which suggests a dimesionless distance between the walls near $a=d_c/L\approx20$. We obtain $\mathrm{Ra}\approx0.05$ using the values found in Wu [26]: $\delta=0.84\times10^{-3}$, $g=980$ cm/s$^2$, and $\nu=9.2\times10^{-3}$ cm$^2$/s. We study the front in the vicinity of these values of Ra and $a$ with different average speeds for the Poiseuille flow.

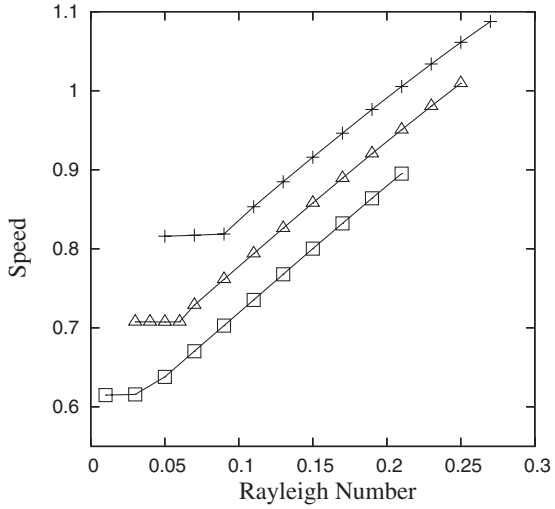


FIG. 1. The dimensionless front speed as a function of the Rayleigh number for different average velocities of the Poiseuille flow ($\bar{V}$). The distance between the walls is $a=20$. The results correspond to the reaction-diffusion-convection equations with viscous boundary conditions. The triangles correspond to no Poiseuille flow (△), the squares (□) to $\bar{V}=-0.1$, and the plus signs (+) to $\bar{V}=0.1$.

The results using the reaction-diffusion-convection equation are shown in Fig. 1, where we display the front speed as a function of Rayleigh number keeping the wall separation at $a=20$. The line corresponding to zero Poiseuille flow shows an increase of speed for Ra numbers above 0.06 which is consistent with our estimates, otherwise the front speed is the convectionless front speed $v_0=1/\sqrt{2}$ [32]. Once Poiseuille flow is turned on we observe a similar increase of speed but at different Rayleigh numbers. We find a sharp increase of speed for $\mathrm{Ra}>0.11$ when the average Poiseuille velocity $\bar{V}$ is +0.1, while the transition takes place when $\mathrm{Ra}>0.04$ in the $\bar{V}=-0.1$ case. This behavior is also reflected in the case of free boundary conditions with the increase of speed occurring at different values of the Rayleigh number as shown in

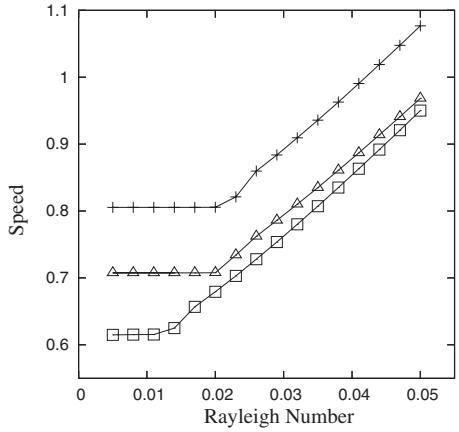


FIG. 2. The dimensionless front speed as a function of the Rayleigh number for different average velocities of the Poiseuille flow ($\bar{V}$). The distance between the walls is $a=20$. The results correspond to the reaction-diffusion-convection equations with free boundary conditions. The triangles correspond to no Poiseuille flow (△), the squares (□) to $\bar{V}=-0.1$, and the plus signs (+) to $\bar{V}=0.1$.

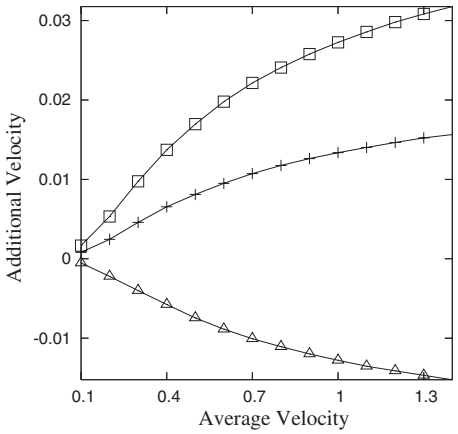


FIG. 3. The additional front velocity due to gravity for advected, axisymmetric fronts. The squares (□) correspond to Ra=0.04, the plus signs (+) to Ra=0.02, and the triangles (△) to Ra=−0.02. The units are the dimensionless units described in the text.

Fig. 2. In this case the transition occurs at Ra$>$0.021 for $\bar{V}=0.1$ and Ra$>$0.011 for $\bar{V}=-0.1$. The fact that the transition takes place at lower values of Ra for free boundaries shows that the viscous boundaries provide additional stability to the front.

For Rayleigh numbers below the transition, the front has a speed close to (but not equal to) the flat front speed plus the corresponding average Poiseuille velocity. The state before the transition cannot be characterized as a convectionless front, since fluid motion due to gravity is always present even before the transition occurs. The reason is that without gravity the Poiseuille flow changes the front curvature depending on the direction of propagation of the front, either with or against the flow. The front curvature caused by the flow results in a horizontal density gradient, which always leads to fluid motion due to gravity regardless of the Rayleigh number. For very small Rayleigh numbers the front is curved having the same symmetry as the front without gravitational effects [41]. The front is symmetric with respect to a line through the center of the two-dimensional domain ($x=a/2$), which we call the axis. The speed of these fronts is affected by the small Rayleigh number. In Fig. 3 we show the change of speed due to a small Rayleigh number for fronts advected by the Poiseuille flow. Here we consider a front that propagates in the same direction as the Poiseuille flow. Figure 3 also shows that increasing the average Poiseuille flow increases the gravitational effects on the front velocity. We also show (Fig. 3) that the increase of speed is larger for larger positive Rayleigh numbers (Ra=0.04 as compared to Ra=0.02). In this figure we also show that a negative Rayleigh number (as in the case of fronts propagating downwards) actually diminishes the additional speed. We point out that in all these cases the additional speed is small compared to the convectionless front speed, roughly less than 4%.

After the transition takes place, the front is no longer axisymmetric. In Fig. 4 we display the fluid velocity described by the stream function $\psi$ which corresponds to the additional velocity on the Poiseuille flow. Here the front propagates upward and the Poiseuille flow ($\bar{V}=-0.1$) is against the direction of propagation. In Fig. 4(a) the Rayleigh number is below the transition, the front is axysimmetric with a velocity field consisting of two rolls, one the mirror image of the other. Here fluid rises along the sides and falls in the middle of the two-dimensional tube. For Ra=0.04, the front is no longer axisymmetric, one of the convective rolls is clearly stronger. There is a stronger upward fluid motion on one side with the downward flow away from the center. For Ra=0.05, the motion consists of a single roll with fluid rising on one side and falling on the other side (Fig. 5).

The results for the front evolution model also exhibit a sharp speed transition as we increase the Rayleigh number. Figures 6 and 7 show the results of the front evolution equation for the two types of boundary conditions: free and viscous boundaries. Figure 6 shows the increase of speed as calculated with free boundaries while Fig. 7 shows the increase of speed using viscous boundaries. For the free

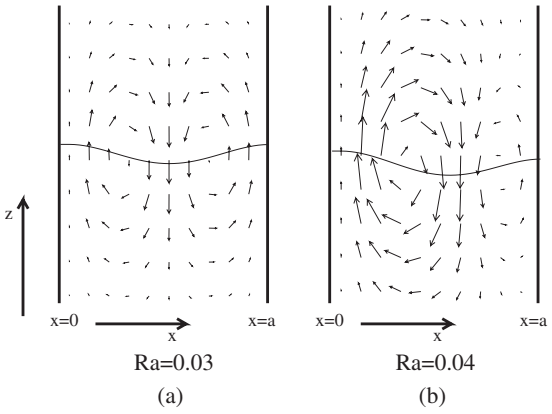


FIG. 4. The additional fluid velocity field near the front. For (a) Ra=0.03 we find an axisymmetric front, while for (b) Ra=0.04 it is no longer axisymmetric.

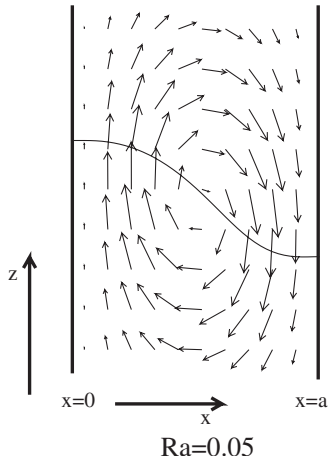


FIG. 5. The additional fluid velocity field near the front for Ra=0.05. Here the front is nonaxisymmetric.

boundary case, we used the Fourier series expansion with ten terms [Eq. (26)], while for viscous boundaries we used the results from the two-term expansion in the stream function [Eqs. (30)–(33)]. We verified that adding terms to the Fourier expansion in the free boundary case does not change the results significantly. Introducing more terms for viscous boundaries is more difficult, since the Fourier series for the front height is not orthogonal to the expansion for the stream function. However, in Ref. [15] additional terms do not alter significantly the linear stability analysis for flat fronts, consequently we expect that the truncations leading to Eqs. (30)–(33) will be sufficient for fronts near the nonaxisymmetric transition. To support these approximations we also

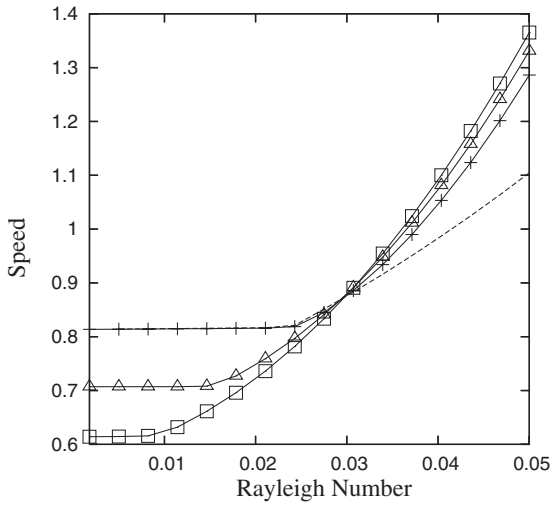


FIG. 6. The speed of the front as a function of the Rayleigh number for different average velocities of the Poiseuille flow. The distance between the walls is $a=20$. The model is the front evolution equations with free boundary conditions. The triangles correspond to no Poiseuille flow (△), the squares (□) to $\bar{V}=-0.1$, and the plus signs (+) to $\bar{V}=0.1$. The dotted line corresponds to the finite difference model. The units are the dimensionless units described in the text.

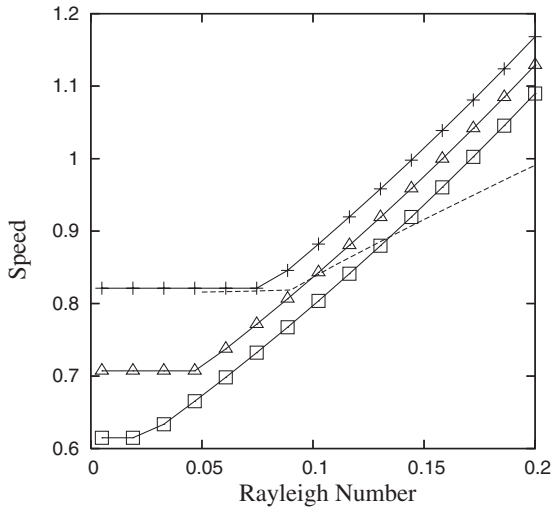


FIG. 7. The speed of the front as a function of the Rayleigh number for different average velocities of the Poiseuille flow. The distance between the walls is $a=20$. The model is the three variable model Eqs. (31)–(33) for viscous boundaries. The triangles correspond to no Poiseuille flow (△), the squares (□) to $\bar{V}=-0.1$, and the plus signs (+) to $\bar{V}=0.1$. The dotted line corresponds to the finite difference model. The units are the dimensionless units described in the text.

display in Figs. 6 and 7 result for the reaction-diffusion model. We display in Fig. 6 the front speed as a function of the Rayleigh number for different Poiseuille flow velocities. We compare the results with the ones obtained using the reaction-diffusion equation. Both models exhibit the transition at the same Rayleigh numbers, but the increase of speed after the transition is somewhat faster using the front-evolution model. We also observe that the three lines after the transition cross each other, which is not the case for the reaction-diffusion model. This may be due to the fact that the front evolution approximation assumes a small curvature, with front curvature increasing significantly after the transition takes place. The results for viscous boundary conditions also show good agreement with the reaction-diffusion results as shown in Fig. 7. In this case we use the truncation defined by Equations (31)–(33). Here we also find a transition to a nonaxisymmetric front with the corresponding sharp increase of speed, but the increase of speed is faster compared to the reaction-diffusion model. The critical Rayleigh numbers obtained with each model are slightly different. Further insights can be gained with the three term truncation by carrying out a linear stability analysis of the initial axisymmetric state. This state is characterized by having $H_1=0$ and $H_2$ being a function of $\bar{V}$ and the Rayleigh number Ra. We carried out a linear stability analysis of Eqs. (32) and (33) to first order on $\bar{V}$ resulting in a relation between the critical Rayleigh number and the dimensionless wall separation $a$,

$$\mathrm{Ra} = \frac{\pi^3}{a^3 f_1} + \frac{6 v_0 \bar{V}}{\pi a (4 f_1 - f_2)}. \tag{34}$$

For $\bar{V}=0$ the critical Rayleigh numbers correspond to previous works [14,15,27]. The parameters $f_1$ and $f_2$ depend on

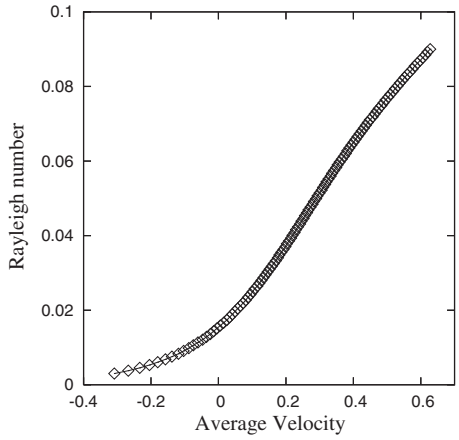


FIG. 8. The critical Rayleigh number for a nonaxisymmetric transition as a function of the dimensionless average velocity of the Poiseuille front.

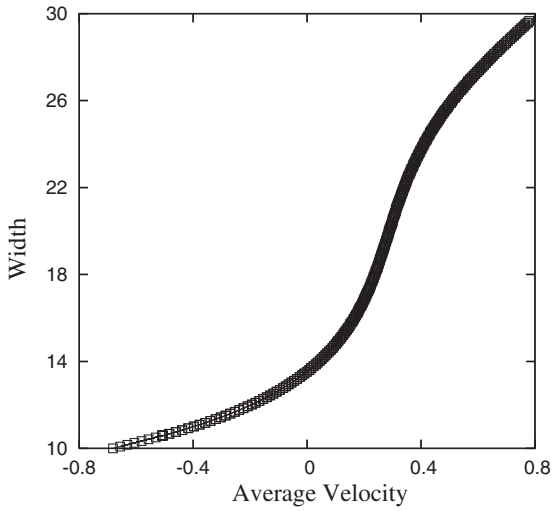


FIG. 9. The critical two-dimensional tube width for a nonaxisymmetric transition as a function of the average velocity of the Poiseuille front. The units are the dimensionless units described in the text.

the type of boundary conditions and they have been defined above. The critical Rayleigh number increases as we increase $\bar{V}$. Previous work showed that the front speed $v_0$ plays a negligible role in the transition to convection for flat fronts due to the large value of the Schmidt number. Here the dimensionless front speed $v_0$ plays an important role when Poiseuille flow is present. If it is neglected there will be no dependence of the critical Rayleigh number with respect to $\bar{V}$.

We use the front evolution with free boundaries to show the dependence of the critical Rayleigh number on the Poiseuille flow velocity (Fig. 7). These results are close to the ones obtained with the reaction-diffusion-convection system (Fig. 2) but with less computational effort. We observe in Fig. 8 that the critical Rayleigh number increases for positive Poiseuille flow speeds, but decreases for negative flow speeds. This suggests a way to experimentally observe the transition. We can start an experiment where the Rayleigh number is just above the critical Rayleigh number, then we can impose a Poiseuille flow to increase the critical Rayleigh number. In this way, the initial front (nonaxisymmetric) will become an axisymmetric front. In Fig. 9 we show the dependence of the critical wall separation with respect to the Poiseuille flow velocity. If the front propagates in a domain where the wall separation is below critical, the front will be axisymmetric, otherwise it will become nonaxisymmetric. Our results show that the critical wall separation increases as the average flow speed increases from $\bar{V}=-0.7$ to $\bar{V}=0.8$. Experiments with different tube diameter were conducted to locate the onset of convection without Poiseuille flow. These experiments in the presence of Poiseuille flow will show the dependence of the critical diameter as a function of $\bar{V}$.

## VI. CONCLUSIONS

In this paper we studied the gravitational effects of chemical fronts advected by a Poiseuille flow caused by the density difference between reacted and unreacted fluid. For small Rayleigh numbers or small wall separations we found that the front deformation always induces flow caused by gravity, resulting in a change of speed for the advected front. As the Rayleigh number or the wall separation is increased, the advected front loses stability to a nonaxisymmetric state, with a consequent sharp increase in front speed. Experiments can locate the critical width for the nonaxisymmetric transition as the front propagates with or against the Pouiseuille front (Fig. 9). This provides more contrasting results than measuring the small change of speed for the initial axisymmetric front (Fig. 3)

The results using the front evolution equation are similar to the ones found for the reaction-diffusion model. One of the advantages of using a front evolution model is that it can be reduced to a simpler three variable model that shows good results. The use of free boundaries provides the same qualitative features for the transition to the nonaxisymmetric state simplifying the equations. Future work should incorporate the corresponding geometry of the experiments, either a three-dimensional cylinder or a Hele-Shaw cell. Our results show that the advected fronts become more stable (higher critical Rayleigh number) as the front propagates in the same direction of the Poiseuille flow. These effects can be measured in experiments using relatively small velocities for the Poiseuille flow.

## ACKNOWLEDGMENT

This work was supported by an award from Research Corporation.

[1] H. Miike, S. C. Müller, and B. Hess, Phys. Lett. A **141**, 25 (1989).
[2] D. Horváth, T. Bánsági, Jr., and A. Tóth, J. Chem. Phys. **117**, 4399 (2002).
[3] T. Bánsági, Jr., D. Horváth, and A. Tóth, Phys. Rev. E **68**, 026303 (2003).
[4] D. A. Vasquez, and A. De Wit, J. Chem. Phys. **121**, 935 (2004).
[5] J. A. Pojman, I. P. Nagy, and I. R. Epstein, J. Phys. Chem. **95**, 1306 (1991).
[6] A. Keresztessy, I. P. Nagy, and J. A. Pojman, J. Phys. Chem. **99**, 5379 (1995).
[7] T. McManus, Ph.D. thesis, West Virginia University (Morgantown, WV), 1989; J. Pojman, I. R. Epstein, T. J. McManus, and K. Showalter, J. Phys. Chem. **95**, 1299 (1991).
[8] J. Masere, D. A. Vasquez, B. F. Edwards, J. W. Wilder, and K. Showalter, J. Phys. Chem. **98**, 6505 (1994).
[9] M. Böckmann and S. C. Müller, Phys. Rev. Lett. **85**, 2506 (2000).
[10] M. R. Carey, S. W. Morris, and P. Kolodner, Phys. Rev. E **53**, 6012 (1996).
[11] J. D'Hernoncourt, A. Zebib, and A. De Wit, Chaos **17**, 013109 (2007).
[12] B. S. Martincigh, C. R. Chinake, T. Howes, and R. H. Simoyi, Phys. Rev. E **55**, 7299 (1997).
[13] B. S. Martincigh and R. H. Simoyi, J. Phys. Chem. A **106**, 482 (2002).
[14] B. F. Edwards, J. W. Wilder, and K. Showalter, Phys. Rev. A **43**, 749 (1991).
[15] D. A. Vasquez, B. F. Edwards, and J. W. Wilder, Phys. Rev. A **43**, 6694 (1991).
[16] J. W. Wilder, B. F. Edwards, and D. A. Vasquez, Phys. Rev. A **45**, 2320 (1992).
[17] H. Wilke, Physica D **86**, 508 (1995).
[18] I. Nagypal, G. Bazsa, and I. R. Epstein, J. Am. Chem. Soc. **108**, 3635 (1986).
[19] T. Plesser, H. Wilke, and K. H. Winters, Chem. Phys. Lett. **200**, 158 (1992).
[20] J. A. Pojman and I. R. Epstein, J. Phys. Chem. **94**, 4966 (1990).
[21] J. A. Pojman, I. R. Epstein, T. J. McManus, and K. Showalter, J. Phys. Chem. **95**, 1299 (1991).
[22] D. A. Vasquez, B. F. Edwards, and J. W. Wilder, Phys. Fluids A **4**, 2410 (1992).
[23] M. C. Rogers and S. W. Morris, Phys. Rev. Lett. **95**, 024505 (2005).
[24] B. F. Edwards, Phys. Rev. Lett. **89**, 104501 (2002).
[25] M. Leconte, J. Martin, N. Rakotomalala, and D. Salin, Phys. Rev. Lett. **90**, 128302 (2003).
[26] Y. Wu, D. A. Vasquez, B. F. Edwards, and J. W. Wilder, Phys. Rev. E **52**, 6175 (1995).
[27] D. A. Vasquez, J. M. Littley, J. W. Wilder, and B. F. Edwards, Phys. Rev. E **50**, 280 (1994).
[28] A. De Wit, Phys. Fluids **16**, 163 (2004).
[29] D. A. Vasquez and E. Thoreson, Chaos **12**, 49 (2002).
[30] J. J. Tyson and J. P. Keener, Physica D **32**, 327 (1988).
[31] R. S. Spangler and B. F. Edwards, J. Chem. Phys. **118**, 5911 (2003).
[32] K. Showalter, Nonlinear Sci. Today **4**, 1 (1995).
[33] J. W. Wilder, B. F. Edwards, D. A. Vasquez, and G. I. Sivashinsky, Physica D **73**, 217 (1994).
[34] J. W. Wilder, D. A. Vasquez, and B. F. Edwards, Phys. Rev. E **56**, 3016 (1997).
[35] D. A. Vasquez, Phys. Rev. E **56**, 6767 (1997).
[36] S. Chandrasekhar, *Hydrodynamic and Hydromagnetic Stability* (Dover, New York, 1981).
[37] P. N. Swarztrauber and R. A. Sweet, ACM Trans. Math. Softw. **5**, 352 (1979).
[38] S. E. Koonin and D. C. Meredith, *Computational Physics (FORTRAN Version)* (Addison-Wesley, Reading, MA, 1990).
[39] C. A. J. Fletcher, *Computational Techniques for Fluid Dynamics*, 2nd ed (Springer-Verlag, New York, 1991).
[40] A. Saul and K. Showalter, in *Oscillations and Traveling Waves in Chemical Systems*, edited by R. J. Field and M. Burger (Wiley, New York, 1985), pp. 419–439.
[41] B. F. Edwards, Chaos **16**, 043106 (2006).